# Multirate Sampled-Data Output Feedback Control With Application to Smart Material Actuated Systems

Jeffrey H. Ahrens, *Member, IEEE*, Xiaobo Tan, *Member, IEEE*, and Hassan K. Khalil, *Fellow, IEEE*

***Abstract*—We consider multirate sampled-data output feedback control of a class of nonlinear systems using high-gain observers where the measurement sampling rate is made faster than the control update rate. We show that, in the presence of bounded disturbances, given a sampled data state feedback controller that achieves stabilization with respect to a closed set, the multirate output feedback controller recovers stabilization of the same set provided the measurement sampling rate is sufficiently fast. As an application we consider the control of smart material actuated systems. This scheme combines a discrete-time high-gain observer with a hysteresis inversion controller where the hysteresis is modeled using a Preisach operator. Experimental results for the control of a shape memory alloy actuated rotary joint are provided.**

***Index Terms*—Hysteresis, multirate, nonlinear observers.**

## I. Introduction

THE study of nonlinear sampled-data systems has received significant attention due to the fact that modern control systems are almost always implemented digitally [4]. See [5], [18], [25], [26] and the references therein for efforts in this direction. There are several approaches to the design of digital controllers. One main approach is the design of a continuous-time controller based on a continuous-time plant model followed by controller discretization. For this design method, stability of the continuous-time plant is typically achieved by choosing a sufficiently small sampling period $T$ [31]. Results on sampled-data output feedback control and digital observers for nonlinear systems can be found in [7], [15], [18], [20], [23], and [29]. In [29], multirate design of a sliding-mode observer is considered where the observer processing rate is higher than the control update rate. In [27], multirate sampled-data stabilization in the presence of time delay was studied for the case when the control rate is made faster than the measurement rate. In [7], a continuous-time state feedback controller is discretized and implemented using a discretized high-gain observer. It was shown that the output feedback controller stabilizes the origin of the closed-loop system for sufficiently small sampling period and recovers the performance under continuous-time state feedback as the sampling period is decreased. For the discretized high-gain observer more accurate estimation of the system states is achieved by faster sampling of the output.

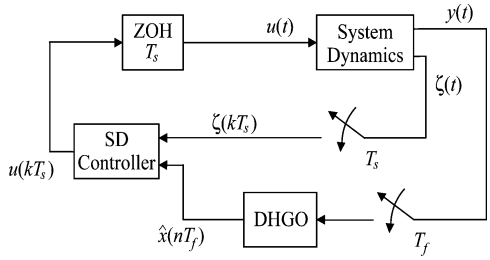


Fig. 1. Diagram of the multirate control scheme showing a sampled-data (SD) controller and discrete-time high-gain observer (DHGO).

In this paper we seek to study the stability of a system under sampled-data output feedback, where the control rate is fixed by the sampled-data state feedback design, while the output sampling rate is faster. The multirate sampled-data output feedback control scheme is illustrated in Fig. 1 for the class of nonlinear systems under consideration (see below). Here we allow two measured outputs $\zeta$ and $y$, of which $y$ will be the driving input of the high-gain observer. We sample the output $\zeta$ with sampling period $T_s$. We apply the control signal at the same rate through a zero-order hold (ZOH) where the control is held constant in between sampling points. The output $y$ is sampled at a faster rate where we use the period $T_f < T_s$. The central contribution of this paper is the demonstration of closed-loop stability for the output feedback system when the measurement sampling rate is made faster than the control update rate. In addition, the inclusion of exogenous signals, which may represent bounded disturbances or reference signals, distinguishes this paper from the results of [7]. Due to the presence of these exogenous signals we consider stabilization with respect to a closed set $\mathcal{A}$ that contains the origin of the closed-loop system. We provide analytical results by showing that with a sampled-data state feedback controller design that achieves stabilization with respect to $\mathcal{A}$, the closed-loop trajectories under the multirate output feedback controller will come arbitrarily close to $\mathcal{A}$. Further, we show that if the closed-loop system under sampled-data state feedback is exponentially stable, then the trajectories of the closed-loop multirate output feedback system will exponentially converge to the origin.

One area of application that may benefit from a multirate control scheme is the case of systems that employ computationally demanding controllers where the control update rate is dictated by the state feedback design. As an example we consider the control of smart material actuated systems that use hysteresis inversion algorithms [30]. In addition to hysteresis, difficulty in

Manuscript received November 11, 2008; revised February 22, 2009. First published October 13, 2009; current version published November 04, 2009. This paper was presented in part at the IEEE American Control Conference, 2007. This work was supported in part by the National Science Foundation under Grants ECS-0114691 and ECS-0400470. Recommended by Associate Editor H. Ito.

J. H. Ahrens is with the Sullivan Park R&D Center, Corning Incorporated, Corning, NY 14870 USA (e-mail: ahrensjh@corning.com).

X. Tan and H. K. Khalil are with the Department of Electrical and Computer Engineering, Michigan State University, East Lansing, MI 48824-1226 USA (e-mail: khalil@egr.msu.edu; xbtan@egr.msu.edu).

Color versions of one or more of the figures in this paper are available online at http://ieeexplore.ieee.org.

Digital Object Identifier 10.1109/TAC.2009.2031204

measuring system states in smart material applications points to output feedback control designs [10].

This paper is organized as follows. In Section II we present the class of nonlinear systems under consideration and derive the closed-loop system under multirate sampled-data output feedback. Section III provides the analytical results where we study the closed-loop stability of the multirate output feedback controller in the presence of bounded disturbances, given a sampled-data state feedback controller that uniformly globally asymptotically stabilizes a set containing the origin. Section IV applies the multirate control scheme to the control of smart material actuated systems and Section V provides some experimental results based on multirate output feedback control of a shape memory alloy actuated rotary joint.

## II. Control Design

### A. Class of Systems

Consider the nonlinear system

$$\dot{z} = g(x, z, d, u) \tag{1}$$

$$\dot{x} = Ax + B\phi(x, z, d, u) \tag{2}$$

$$y = Cx \tag{3}$$

$$\zeta = \Theta(x, z, d) \tag{4}$$

where $x \in \mathbb{R}^r$ and $z \in \mathbb{R}^s$ are the states, $u \in \mathbb{R}$ is the input, $y \in \mathbb{R}$ and $\zeta \in \mathbb{R}^m$ are the measured outputs, and $d(t) \in \mathbb{R}^d$ is vector of exogenous signals. The $r \times r$ matrix $A$, the $r \times 1$ matrix $B$, and the $1 \times r$ matrix $C$ are given by

$$A = \begin{bmatrix} 0 & 1 & \dots & \dots & 0 \\ 0 & 0 & 1 & \dots & 0 \\ \vdots & & & & \vdots \\ 0 & \dots & \dots & 0 & 1 \\ 0 & 0 & \dots & \dots & 0 \end{bmatrix}, \quad B = \begin{bmatrix} 0 \\ 0 \\ \vdots \\ 0 \\ 1 \end{bmatrix}$$

$$C = [1 \quad 0 \quad \dots \quad \dots \quad 0].$$

*Assumption 1:*

1) $d(t)$ is continuously differentiable, $d(t)$ and $\dot{d}(t)$ are bounded, and $d(t)$ takes values in the compact set $\mathcal{D}$.
2) The functions $\phi$: $\mathbb{R}^r \times \mathbb{R}^s \times \mathbb{R}^d \times \mathbb{R} \to \mathbb{R}$, $g$: $\mathbb{R}^r \times \mathbb{R}^s \times \mathbb{R}^d \times \mathbb{R} \to \mathbb{R}^s$, and $\Theta$: $\mathbb{R}^r \times \mathbb{R}^s \times \mathbb{R}^d \to \mathbb{R}^m$ are locally Lipschitz in their arguments, uniformly in $d$, over the domain of interest.

One source for the model (1)–(4) is the normal form of input-output linearizable systems, as discussed in [17]. In addition to the normal form, this class of systems also arises in mechanical and electromechanical systems where the position is measured, but its derivatives, the velocity and acceleration, are not measured. The high-gain observer takes the form

$$\dot{\hat{x}} = A\hat{x} + B\phi_0(\hat{x}, \zeta, d, u) + H(y - C\hat{x}) \tag{5}$$

where $\hat{x}$ is the estimate of the state $x$ and $\phi_0$ is a nominal model of $\phi$. The gain matrix is given by

$$H^T = \left[\frac{\alpha_1}{\varepsilon} \; \frac{\alpha_2}{\varepsilon^2} \; \cdots \; \frac{\alpha_r}{\varepsilon^r}\right]$$

where $\varepsilon$ is a small positive parameter and the roots of $s^r + \alpha_1 s^{r-1} + \cdots + \alpha_{r-1}s + \alpha_r = 0$ have negative real parts.

*Assumption 2:* The function $\phi_0$ is locally Lipschitz in its arguments, uniformly in $d$, over the domain of interest, and globally bounded in $\hat{x}$.

The global boundedness in $\hat{x}$ can always be achieved by saturation outside a compact set of interest. It is required to overcome peaking in the transient behavior of the high-gain observer [11].

To study the closed-loop system under multirate output feedback control, we need a description of the system dynamics in discrete-time. Rewrite (1) and (2) as

$$\dot{\chi} = f(\chi, d, u) \tag{6}$$

where $\chi = (z, x) \in \mathbb{R}^{s+r}$ and

$$f(\chi, d, u) = \begin{bmatrix} g(x, z, d, u) \\ Ax + B\phi(x, z, d, u) \end{bmatrix}.$$

The control $u$ is applied to the system through a zero-order hold, thus it is held constant in between sampling points. In what follows, we will allow the discrete-time control to be corrupted by a bounded disturbance $e$ that takes values in the known compact set $\mathcal{E} \subset \mathbb{R}$. In Section IV, when we consider applications to smart material systems this disturbance will result from hysteresis inversion error. For now, the control $u$ will be taken as the synthesized control $u_e$ plus a general disturbance

$$u(k) = u_e(k) + e(k)$$

where the discrete-time index $k$ denotes the $k$th sampling instant $t = kT_s$. The solution of (6) over the sampling period $[kT_s, kT_s + T_s]$ is given by

$$\chi(t) = \chi(k) + (t - kT_s) f(\chi(k), d(k), u(k)) + \int_{kT_s}^{t} [f(\chi(\tau), d(\tau), u(k)) - f(\chi(k), d(k), u(k))]\, d\tau. \tag{7}$$

By adding and subtracting terms to the integral and using the Lipschitz property of the function $f$ we can arrive at

$$\|\chi(t) - \chi(k)\| \le (t - kT_s)\|f(\chi(k), d(k), u(k))\| + L_1 \int_{kT_s}^{t} \|\chi(\tau) - \chi(k)\| d\tau + L_2 \int_{kT_s}^{t} \|d(\tau) - d(k)\| d\tau$$

where $L_1$ and $L_2$ are Lipschitz constants of $f$ with respect $\chi$ and $d$, respectively, for all $d \in \mathcal{D}$ and all $\chi$ belonging to the compact set $\Omega_2^s$ that will be determined shortly. From Assumption 1 this simplifies to

$$\|\chi(t) - \chi(k)\| \le (t - kT_s)\|f(\chi(k), d(k), u(k))\| + L_3(t - kT_s)^2 + L_1 \int_{kT_s}^{t} \|\chi(\tau) - \chi(k)\| d\tau$$

for some positive constant $L_3$. Applying the Gronwall-Bellman lemma to the above equation results in the inequality

$$\|\chi(t) - \chi(k)\| \le \frac{1}{L_1}\left[e^{(t-kT_s)L_1} - 1\right] \times \|f(\chi(k), d(k), u(k))\| + \frac{2L_3}{L_1^2} \times \left[e^{(t-kT_s)L_1} - L_1(t - kT_s) - 1\right]. \tag{8}$$

Based on the foregoing, we may describe the dynamics of the system (6) at the sampling points by the following discrete-time equation:

$$\chi(k+1) = \chi(k) + T_s f(\chi(k), d(k), u(k))$$

$$+T_s^2\Phi_d(k,\chi(k),u(k),T_s) \quad (9)$$

where the integral term in (7), with dependence on the exogenous signal $d$, is captured by the time-varying function $\Phi_d$. Furthermore, $\Phi_d$ is bounded uniformly in $T_s$, for $T_s$ sufficiently small, on compact sets of $(\chi,u)$. This model and (8) describe the discrete-time plant dynamics and the intersampling behavior, respectively. We consider a discrete-time dynamic controller based on single-rate state feedback

$$\vartheta(k+1)=\Lambda(\vartheta(k),x(k),\zeta(k),d(k)) \quad (10)$$

$$u_e(k)=\gamma(\vartheta(k),x(k),\zeta(k),d(k)) \quad (11)$$

where $\vartheta\in\mathbb{R}^p$.

*Assumption 3:*

1) The functions $\gamma$ and $\Lambda$ are locally Lipschitz in their arguments, uniformly in $d$, over the domain of interest.
2) $\gamma$ and $\Lambda$ are globally bounded functions of $x$.

To simplify the presentation let $\chi_a=(\vartheta,\chi)$, where $\chi_a\in\mathbb{R}^\ell$ and $\ell=p+s+r$. Next augment the discrete-time system (9) with (10)

$$\mathcal{F}(k,\chi_a(k),x(k),d(k),u(k),T_s)\stackrel{def}{=}\begin{bmatrix}\Lambda(\vartheta(k),x(k),\zeta(k),d(k))\\ \chi(k)+T_sf(\chi(k),d(k),u(k))+T_s^2\Phi_d(k,\chi(k),u(k),T_s)\end{bmatrix}.$$

Using (11) the closed-loop system under slow sampled-data state feedback can be written as

$$u_e(k)=\gamma(\vartheta(k),x(k),\zeta(k),d(k)) \quad (12)$$

$$\chi_a(k+1)=\mathcal{F}(k,\chi_a(k),x(k),d(k),u_e(k)+e(k),T_s). \quad (13)$$

Due to the presence of the bounded error $e$ and the exogenous signal $d$, we assume the existence of a single-rate sampled-data state feedback controller that renders a closed set containing the origin uniformly globally asymptotically stable (UGAS). We work with the notion of UGAS found in [16]. Let $\mathcal{A}$ be a closed subset of $\mathbb{R}^\ell$ that contains the origin. The size of $\mathcal{A}$ depends on the size of the signals $e$ and $d$. The distance of a point $\chi_a\in\mathbb{R}^\ell$ to the set $\mathcal{A}$ is given by

$$|\chi_a|_{\mathcal{A}}=\inf_{\eta\in\mathcal{A}}\|\chi_a-\eta\|. \quad (14)$$

With this definition the closed-loop state feedback system is UGAS with respect to $\mathcal{A}$ if and only if there exists a class $\mathcal{KL}$ function $\beta$ such that the solution of (12)–(13), $\chi_a(k)$, which depends on the initial state $\chi_a(0)$, $d$, and $e$, satisfies $|\chi_a(k)|_{\mathcal{A}}\le\beta(|\chi_a(0)|_{\mathcal{A}},k)$ for all $k\ge0$, $\chi_a(0)\in\mathbb{R}^\ell$, $d\in\mathcal{D}$, and $e\in\mathcal{E}$. We state our assumptions on the closed-loop single-rate state feedback system.

*Assumption 4:* The closed-loop sampled-data state feedback system (12)–(13) is UGAS with respect to the closed set $\mathcal{A}$ and there exist a function $V$ (dependent on $T_s$), class $\mathcal{K}_\infty$ functions $U_1$ and $U_2$ (independent of $T_s$), a continuous positive definite function $U_3$ (dependent on $T_s$), and a constant $T_s^*>0$ such that the following inequalities hold:

$$U_1(|\chi_a|_{\mathcal{A}})\le V(k,\chi_a)\le U_2(|\chi_a|_{\mathcal{A}}) \quad (15)$$

$$V(k+1,\mathcal{F}(k,\chi_a,x,d,\gamma(\vartheta,x,\zeta,d)+e,T_s))-V(k,\chi_a)\le-U_3(|\chi_a|_{\mathcal{A}}) \quad (16)$$

for all $0<T_s\le T_s^*$.

*Remark 1:* We note that for UGAS discrete-time systems with disturbances, Theorem 1 of [16] guarantees the existence of a smooth Lyapunov function $V(k,\chi_a)$ that depends on $T_s$ and satisfies (15)–(16). Assumption 4 is a bit stronger in that we require the functions $U_1$ and $U_2$ to be independent of $T_s$. Further, due to the difficulty in computing exact discrete-time models for nonlinear systems we note that the function $\Phi_d$ in (9) is typically unknown. Assumption 4 may be satisfied by applying the results of [24], [25], and [26]. In [24] sufficient conditions are given to show stability of an exact discrete-time plant model based on a controller that stabilizes an approximate discrete-time nonlinear model using the notion of Lyapunov semiglobal practical input-to-state stability (SP-ISS). Under SP-ISS, the class $\mathcal{K}_\infty$ functions that bound the Lyapunov function are allowed to be independent of the sample time.

As mentioned in the introduction, in the design of discrete-time controllers, boundedness of the trajectories of the continuous-time plant is typically provided by choosing the sampling period $T_s$ small enough. This can be demonstrated by considering the Lyapunov function $V(k,\chi_a(k))$. We note that for any $c_2^s>c_1^s>0$ the sets

$$\Omega_1^s=\{V(k,\chi_a(k))\le c_1^s\}\subset\Omega_2^s=\{V(k,\chi_a(k))\le c_2^s\} \quad (17)$$

are compact subsets of $\mathbb{R}^\ell$. From (15)–(16) we have that any $\chi_a(k)$ that starts in $\Omega_1^s$ will remain in $\Omega_1^s$ for all $k\ge0$, therefore $(\vartheta,x,z)$ are bounded. Using this fact, the Lipschitz continuity property of $\gamma$ and $\Theta$, and the boundedness of $e$ and $d$ it follows that $u$ is bounded. Let $K_u$ be a positive constant independent of $T_s$ such that $\|u\|\le K_u$ for all $k\ge0$. Further, let $L_1$ be a Lipschitz constant of $f$ with respect to $\chi$ over the compact set $\Omega_2^s\times\{\|u\|\le K_u\}$. The sampling period $T_s$ can be chosen small enough that $\chi(t)$ will always remain in $\Omega_2^s$. Indeed, for $\chi_a(k)\in\Omega_1^s$ and $\|u\|\le K_u$ we can use (8) to show that $\|\chi(t)-\chi(k)\|\le\delta(T_s)$ where $\delta(T_s)\to0$ as $T_s\to0$. Thus, in the sampled-data state feedback design, $T_s$ can be chosen so that $\chi(t)$ will be bounded.

The discretized high-gain observer is implemented by first scaling the observer states according to $q=D\hat{x}$ where $D=diag[1,\varepsilon,\ldots,\varepsilon^{r-1}]$. This yields

$$\dot{q}=\frac{1}{\varepsilon}[A_oq+H_oy+\varepsilon^rB\phi_0(D^{-1}q,\zeta,d,u_e)] \quad (18)$$

where $A_o=\varepsilon D(A-HC)D^{-1}=A-H_oC$ and $H_o=\varepsilon DH=[\alpha_1,\ \alpha_2,\ \ldots,\ \alpha_r]^T$. With this scaling, the right-hand side of (18) is of the order $1/\varepsilon$, compared with $1/\varepsilon^r$ in (5). Equation (18) is discretized using the forward difference method. For the dynamics under fast sampling we use the index $n$ to indicate the sampling points that are equally spaced with period $T_f$. We obtain

$$q(n+1)=A_fq(n)+B_fy(n)+\varepsilon^{r-1}T_fB\phi_0\times(D^{-1}q(n),\zeta(k),d(k),u_e(k)) \quad (19)$$

$$\hat{x}(n)=C_fq(n) \quad (20)$$

where $A_f=I+T_fA_o/\varepsilon$, $B_f=T_fH_o/\varepsilon$, and $C_f=D^{-1}$. We point out that $u(k)$, $\zeta(k)$, and $d(k)$ evolve in the slow sampling time $k$ and are constant for all $n$ where $nT_f\in[kT_s,kT_s+T_s)$. The dependence of $\phi_0$ on $d$ in (18) and $d(k)$ in (19) allows for

the possibility that components of these exogenous signals may be measurable or available online, as it is the case with reference signals. If they are not available, as in the case with unmeasurable disturbances, we may simply omit them in the nominal model $\phi_0$. As in [7] we take $T_f = \varepsilon\alpha$ where $\alpha$ is a positive constant chosen such that the matrix $A_f$ has all its eigenvalues inside the unit circle. We choose $T_f$ such that the ratio $T_s/T_f$ of the slow and fast sample rates is a positive integer. The observer estimates are downsampled for use in the output feedback controller. Letting $h = T_s/T_f$ we denote the estimates under the slow sampling period by $\hat{x}_s(k) = \hat{x}(hk)$. This gives the following output feedback controller:

$$\vartheta(k+1) = \Lambda(\vartheta(k), \hat{x}_s(k), \zeta(k), d(k)) \tag{21}$$

$$u_e(k) = \gamma(\vartheta(k), \hat{x}_s(k), \zeta(k), d(k)). \tag{22}$$

The idea of globally bounding the control outside a compact region of interest to overcome the peaking phenomenon was studied in [11]. As discussed in [18], peaking in the initial time instant can be overcome by setting the initial control to some arbitrary values and then using the observer estimates after they have recovered from peaking. We take a similar approach here by using the control

$$\left.\begin{array}{rll} u_e(k) = u_{e0}(k), & \text{for} & 0 \le k < k_0 \\ u_e(k) = \gamma(\vartheta(k), \hat{x}_s(k), \zeta(k), d(k)), & \text{for} & k \ge k_0 \end{array}\right\}. \tag{23}$$

Because of the flexibility of the multirate scheme, we can choose the output sampling rate sufficiently fast so that the estimates recover from peaking during the period $[0, T_s]$. In this case we only have to set the control to some initial value $u_e(0) = u_{e0}$. Furthermore, the states of the plant $\chi(t)$ will not grow by more than $O(T_s)$ from its initial condition during this period. However, the control still needs to be globally bounded to prevent any peaking that occurs after the initial time. Still, the control scheme (23) prevents controller saturation during the peaking period. We will proceed with an arbitrary $k_0$. In the forthcoming analysis we need a model that describes the observer error dynamics. The derivation of such a model is similar to [7] and is omitted here due to space limitations. It uses the relations $DB = \varepsilon^{r-1}B$, $CD = C$, $\varepsilon^i DA^i = A^i D$, $A^r = 0$ and the scaled estimation error

$$\xi(n) = \frac{1}{\varepsilon^{r-1}}\left[D(x(n) - \hat{x}(n)) - MDx(n)\right] \tag{24}$$

where $M$ satisfies the equation $A_f M + (e^{A\alpha} - I - \alpha A) - Me^{A\alpha} = 0$ and the term $-MDx(n)$ is used to eliminate terms in the estimation error that appear with negative powers of $\varepsilon$. Rearranging (24) we have the state estimate $\hat{x}$ given by

$$\hat{x}(n) = [I - \varepsilon N_2(\varepsilon)]x(n) + N_1(\varepsilon)\xi(n) \tag{25}$$

where $N_1(\varepsilon) = -\varepsilon^{r-1}D^{-1}$ and $N_2(\varepsilon) = (1/\varepsilon)D^{-1}MD$ are analytic functions of $\varepsilon$. It can be shown that $\xi(n)$ satisfies the equation

$$\begin{aligned}\xi(n+1) &= A_f\xi(n) \\ &\quad + \varepsilon\mathcal{G}_d(n, \chi(n), \xi(n), d(k), \zeta(k), u_e(k) + e(k), \varepsilon)\end{aligned} \tag{26}$$

where $A_f$ has all its eigenvalues inside the unit circle and $\mathcal{G}_d$, with dependence on $d$, is a time-varying function that is locally Lipschitz in its arguments, uniformly bounded in $\varepsilon$, for $\varepsilon$ sufficiently small, and globally bounded in $\hat{x}$. Also, the control $u_e(k)$ is taken from (23). Together with (26) the closed-loop system under multirate output feedback control is given by

$$u_e(k) = \gamma(\vartheta(k), \hat{x}_s(k), \zeta(k), d(k)) \tag{27}$$

$$\begin{aligned}\chi_a(k+1) &= \mathcal{F}(k, \chi_a(k), \hat{x}_s(k), d(k), u_e(k) \\ &\quad + e(k), T_s)\end{aligned} \tag{28}$$

$$\hat{x}_s(k) = [I - \varepsilon N_2(\varepsilon)]x(k) + N_1(\varepsilon)\xi_s(k) \tag{29}$$

where (29) describes the state estimates under the slow sample period with $\xi_s(k) = \xi(hk)$. Notice that by setting $\varepsilon = 0$ and $\xi_s = 0$ in (29) we have $\hat{x}_s = x$ and thus (28) becomes identical to the slow sampled-data state feedback system (12)–(13).

## III. Main Results

In this section we present stability results for the closed-loop system under multirate output feedback control. Our first result shows that the trajectories of the closed-loop system under multirate output feedback are bounded and ultimately bounded. The proof is given in Appendix I.

*Theorem 1:* Consider the closed-loop system under multirate output feedback (26)–(29). Let Assumptions 1–4 hold and let $\mathcal{M}$ and $\mathcal{N}$ be any compact subsets of $\mathbb{R}^\ell$ and $\mathbb{R}^r$, respectively. Then, for trajectories $\chi_a \times \hat{x}$ starting in $\mathcal{M} \times \mathcal{N}$ the following holds

- There exist $\varepsilon_1^* > 0$ such that for all $0 < \varepsilon \le \varepsilon_1^*$, $\chi_a(k)$ and $\xi(n)$ are bounded for all $k \ge 0$ and all $n \ge 0$.
- Given any $\nu \ge 0$, there exists $\varepsilon_2^* > 0$, $k_1^* > 0$, and $n_1^* > 0$, such that for every $0 < \varepsilon \le \varepsilon_2^*$, we have

$$\|\xi(n)\| + |\chi_a(k)|_{\mathcal{A}} \le \nu \;\forall\, k \ge k_1^*, \quad \textit{and} \quad n \ge n_1^* \tag{30}$$

- Given $T_s^* > 0$ designed so that $\chi(t)$ under sampled-data state feedback (10)–(11) is bounded in $\Omega_2^s$ of (17) then, for all $0 < T_s \le T_s^*$ the continuous-time trajectories $\chi(t)$ under multirate output feedback are bounded for all $t \ge 0$ and satisfy

$$\|\chi(t) - \chi(k)\| \le \delta(T_s) \tag{31}$$

where $\delta(T_s) \to 0$ as $T_s \to 0$.

*Remark 2:* The above result covers the regulation and tracking problems in the presence of bounded disturbances. In Assumption 1 we assume that the derivative of the exogenous signal $d$ is bounded as well. This assumption is satisfied for reference trajectories that have been appropriately smoothed by filtering. Otherwise, it may be possible to relax this assumption by applying the results of [20]. We note that in the tracking problem formulation, the state $x$ represents the tracking error. Stabilization of the origin is a special case when the set $\mathcal{A}$ is the origin. In this case Theorem 1 shows boundedness and ultimate boundedness of the trajectories of the closed-loop multirate output feedback system.

*Remark 3:* Comparison of Theorem 1 with the single-rate results of [7] shows that in addition to the multirate output feedback design scheme we have included bounded disturbances and exogenous signals. This analysis is useful when considering tracking problems and applications where plant nonlinearities cannot be exactly canceled.

Under stronger conditions on the closed-loop system we may show that the trajectories converge to the origin. With $d = 0$

and $e = 0$ then $u(k) = u_e(k)$ and the closed-loop system under multirate output feedback can be written as

$$\vartheta(k+1) = \Lambda(\vartheta(k), \hat{x}_s(k), \zeta(k)) \tag{32}$$

$$\chi(k+1) = \chi(k) + T_s f(\chi(k), 0, u(k)) + T_s^2 \Phi_0(\chi(k), u(k), T_s) \tag{33}$$

$$\xi(n+1) = A_f \xi(n) + \varepsilon \mathcal{G}_0(\chi(n), \xi(n), 0, \zeta(k), u(k), \varepsilon) \tag{34}$$

$$\hat{x}_s(k) = [I - \varepsilon N_2(\varepsilon)] x(k) + N_1(\varepsilon) \xi_s(k) \tag{35}$$

where the function $\Phi_0$ is uniformly bounded in $T_s$, for $T_s$ sufficiently small, and the control scheme is taken from (23) with $u(k) = \gamma(\vartheta(k), \hat{x}_s(k), \zeta(k))$. The single-rate state feedback system for this case can be expressed as

$$\vartheta(k+1) = \Lambda(\vartheta(k), x(k), \zeta(k)) \tag{36}$$

$$\chi(k+1) = \chi(k) + T_s f(\chi(k), 0, u(k)) + T_s^2 \Phi_0(\chi(k), u(k), T_s) \tag{37}$$

where the control $u(k) = \gamma(\vartheta(k), x(k), \zeta(k))$. Under the assumption that the functions $f$, $\Lambda$, and $\gamma$ are continuously differentiable and the origin of the single-rate state feedback system (36)–(37) is locally exponentially stable we can show that the trajectories of the multirate output feedback system (32)–(35) converge to the origin exponentially fast. We state this result in the following theorem; the proof is given in Appendix II.

*Theorem 2:* Consider the closed-loop system under multirate output feedback (32)–(35) and the control (23) with $u(k) = \gamma(\vartheta(k), \hat{x}_s(k), \zeta(k))$. Suppose the origin $((\chi, \vartheta) = 0)$ of (36)–(37) is exponentially stable and the functions $f(\chi, 0, u)$, $\Lambda(\vartheta, x, \zeta)$, and $\gamma(\vartheta, x, \zeta)$ are continuously differentiable in a neighborhood of the origin. Let Assumptions 1–3 hold and let $\mathcal{M}$ and $\mathcal{N}$ be any compact subsets of $\mathbb{R}^\ell$ and $\mathbb{R}^r$, respectively. Then, for trajectories $(\vartheta, \chi) \times \hat{x}$ starting in $\mathcal{M} \times \mathcal{N}$ there exists $\varepsilon_3^* > 0$ such that for all $0 < \varepsilon \leq \varepsilon_3^*$ the trajectories of the discrete-time system (32)–(35) converge to the origin exponentially fast in the slow sample time $k$ and the continuous-time trajectory $\chi(t)$ decays to zero, exponentially fast, as $t \to 0$.

## IV. Application to Smart Material Systems

A single-rate output feedback control scheme using high-gain observers may require elevated sampling rates for the entire controller, control and estimation. The multirate scheme may have computational advantage by processing the control at a rate designed under state feedback and only increasing the sampling rate of the estimation. Thus, from a practical point of view the multirate scheme may be more cost effective. This may prove useful in applications that require computationally demanding controllers such as model-based control. Furthermore, the stability results in the presence of bounded disturbances of the previous section may be useful in designs where the controller contains an inexact plant model that is used to cancel plant nonlinearities. This brings us to the current section where we consider an application of the multirate scheme to the control of smart material actuated systems. The actuator model we use is shown in the dotted box of Fig. 2. It is comprised of a hysteresis operator, denoted by $\Gamma$, in cascade with linear dynamics $G(s)$. Smart material actuator models of this form are discussed in [6] and [32]. The input to the hysteresis operator is the signal

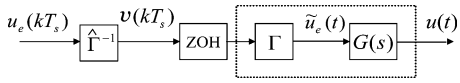


Fig. 2. Diagram of the hysteresis inversion compensation. The smart material actuator model appears in the dotted box.

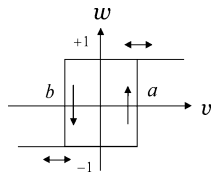


Fig. 3. Delayed relay.

$v$ that is generated by the controller. The output of the actuator, namely, $u$ is the input to the plant we wish to control. We allow this actuator to drive a nonlinear plant of the form (1)–(4). The control scheme will employ a sampled-data controller $u_e$ followed by an inversion operator $\hat{\Gamma}^{-1}$ to cancel the effect of the hysteresis as shown in Fig. 2. This inversion is subject to modeling error and the sampled-data controller is designed to stabilize the system dynamics in the presence of this error. The control update rate $T_s$ will be fixed by the sampled-data state feedback design using hysteresis inversion. We model the hysteresis using a Preisach operator, which is briefly reviewed here. A more detailed discussion is given in [22] and [33]. The Preisach operator is comprised of delayed relay elements $\hat{\gamma}_{(b,a)}$ called hysterons. The switching thresholds of these elements are denoted by $(b, a)$ as shown in Fig. 3. The output of the hysteron is described by $w(t) = \hat{\gamma}_{(b,a)}[v, \varsigma], \forall t \in [0, T]$, where $v$ is a continuous function on $[0, T]$ and $\varsigma \in \{-1, 1\}$ is an initial configuration. The Preisach operator can be described as a weighted superposition of all hysterons. Define the *Preisach plane* as $\mathcal{P}_0 \stackrel{def}{=} \{(b, a) \in \mathbb{R}^2 : b \leq a\}$. Each pair $(b, a)$ is identified with the hysteron $\hat{\gamma}_{(b,a)}$. The output of the Preisach operator is given by

$$\Gamma[v, \varsigma_0](t) = \int_{\mathcal{P}_0} \mu(b, a) \hat{\gamma}_{(b,a)}[v, \varsigma_0](t) db\, da \tag{38}$$

where the weighting $\mu$ is called the *Preisach density* and $\varsigma_0$ is an initial configuration of all hysterons. It is assumed that $\mu \geq 0$ and $\mu(b, a) = 0$ if $b < b_0$ or $a > a_0$ for some $b_0, a_0$. Consider the finite triangular area $\mathcal{P} \stackrel{def}{=} \{(b, a) \in \mathcal{P}_0 | b \geq b_0, a \leq a_0\}$. At any time $t$, we can divide $\mathcal{P}$ into two regions, $\mathcal{P}_+$ and $\mathcal{P}_-$, where $\mathcal{P}_+$ ($\mathcal{P}_-$, resp.) consists of points $(b, a)$ such that $\hat{\gamma}_{(b,a)}$ at time $t$ is $+1$ ($-1$, resp.). The boundary between $\mathcal{P}_+$ and $\mathcal{P}_-$ is called the memory curve, which characterizes the memory of the Preisach operator. The set of all memory curves is denoted by $\Psi$ and $\psi_0$, corresponding to $\varsigma_0$, is called the initial memory curve. In this paper we will make use of the following properties of the Preisach operator.

*Theorem 3: [33]:* Let $v$ be continuous on $[0, T]$ and $\psi_0 \in \Psi$.

1) (Rate Independence) If $\theta : [0, T] \to [0, T]$ is an increasing continuous function, $\theta(0) = 0$, and $\theta(T) = T$, then $\Gamma[v(\theta(t)), \psi_0](t) = \Gamma[v, \psi_0](\theta(t)), \forall t \in [0, T]$.
2) (Piecewise Monotonicity) If $v$ is either nondecreasing or nonincreasing on some interval in $[0, T]$, then so is $\Gamma[v, \psi_0]$.

The hysteresis nonlinearity can be identified by discretizing the input range into $L$ uniform intervals, which generates a discretization grid on the Preisach plane. The Preisach operator can then be approximated by assuming that inside each cell of the grid, the Preisach density function is constant. This piecewise constant approximation to an unknown density function can be found by identifying the weighting masses for each cell using a constrained least squares algorithm and then distributing each mass uniformly over the corresponding cell [30]. We consider a discretization of level $L$ of the Preisach operator. Also, let the Preisach density function $\mu$ be nonnegative and constant within each cell. Given an initial memory curve $\psi_0$ and a desired value $u_e$, the inversion problem is to find a value $v$ such that $u_e = \Gamma[v, \psi_0]$. This is done by applying the algorithm given in [30]. The inversion error of the Preisach operator can be quantified in terms of the level discretization approximation and the error in identifying the weighting masses. Indeed, let

$$v = \hat{\Gamma}^{-1}[u_e, \psi_0] \tag{39}$$

$$\tilde{u}_e = \Gamma[v, \psi_0] \tag{40}$$

as shown in Fig. 2. The control signal $v$ is applied to the system through a zero-order hold. Also, due to the rate independence of the Preisach operator, $\tilde{u}_e$ will be constant in between sampling points. We denote the signal at the $k$th sampling point by $\tilde{u}_e(k) = u_e(k) + e_i(k)$. The inversion error is defined by

$$e_i(k) \stackrel{def}{=} \tilde{u}_e(k) - u_e(k). \tag{41}$$

The signal $u_e$ is designed under sampled-data state feedback and takes the form of (10)–(11). Given a bounded sequence $u_e$ it can be shown ([30]) that the inversion error satisfies a bound of the form

$$\|e_i\|_\infty \leq C_s \delta_i + \frac{k_1}{L} \tag{42}$$

for some positive constant $k_1$, where $\delta_i$ is the error in identification of the weighting masses and $C_s$ is the saturation of the hysteresis. Saturation is common in smart materials. For example, magnetostrictives exhibit magnetization saturation and shape memory alloys exhibit strain saturation. Equation (42) shows that the inversion error decreases with decreasing identification error and with ever-finer discretization grids (increasing the level $L$). Based on this quantification of the upper bound on the inversion error, we have that $e_i$ belongs to a known compact set which we denote $\mathcal{E} \subset \mathbb{R}$. Thus, in the presence of the bounded hysteresis inversion error $e_i$ we consider stabilization of a closed set $\mathcal{A}$ that contains the origin and whose size is determined by $e_i$. Now, consider the plant (1)–(4) as the system that is driven by the smart material actuator. We can absorb the actuator dynamics $G(s)$ into the internal dynamic (1). Then using (39), (40), and (41) we obtain the following equivalent system that is subject to hysteresis inversion error:

$$\dot{z} = g(x, z, d, u_e + e_i) \tag{43}$$

$$\dot{x} = Ax + B\phi(x, z, d) \tag{44}$$

$$y = Cx \tag{45}$$

$$\zeta = \Theta(x, z, d). \tag{46}$$

Thus, with a single-rate partial state feedback control $u_e$, designed with sample period $T_s$, that renders a closed set containing the origin uniformly globally asymptotically stable we can design a discrete-time high gain observer (19)–(20) with fast sampling period $T_f < T_s$ to achieve closed-loop stability of the output feedback system. Indeed, this output feedback control takes the form (21)–(22). Next, we provide experimental results to illustrate the idea.

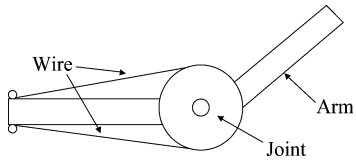


Fig. 4. Robotic joint actuated by two SMA wires.

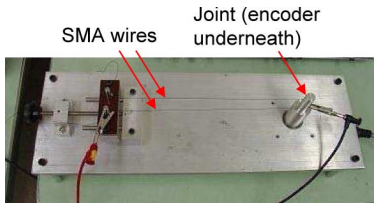


Fig. 5. Picture of the SMA actuated robotic joint setup.

## V. Experimental Results

In this section, we apply multirate output feedback control to a shape memory alloy (SMA) actuated robotic joint. SMAs are metallic materials that exhibit coupling between thermal and mechanical energy domains. The *shape memory effect* (SME) results from a transition between two structural phases that is hysteretic in nature. For more detailed information on the SME consult [9]. The name shape memory results from the material's ability to "remember" an initial shape. For example, SMA wire can be stretched and upon heating the wire, it will contract back to its initial shape. Thus, this thermal/mechanical coupling has motivated the use of SMA as an actuator. Control of shape memory alloy actuated systems can be found in [3], [8], [10], and [14]. Also, control and modeling of hysteresis in SMA has been considered in [12], [13], [21], and [35]. Fig. 4 shows a diagram of the rotary joint. The picture in Fig. 5 illustrates the experimental setup which is similar to the setup used in [12]. This two-wire configuration is referred to as a *differential-type* actuator (see [12]–[14]). The rotating joint consists of a 0.5 inch diameter shaft and two Nitinol wires 10 inches in length and 0.008 inches in diameter. These wires are stretched by 2% of their length. Alternate heating and cooling of the two wires provides clockwise (CW) and counterclockwise (CCW) rotation. With this configuration the actuator can achieve up to 60 degrees rotation in each direction. Bipolar current is supplied to the actuator where positive current gives CW rotation by heating one wire and negative current gives CCW rotation by heating the other. The joint rotation angle is obtained through an 8192 counts/rev incremental encoder.

For these experiments, we use a model similar to the one shown in Fig. 2. A Preisach operator is used to capture the nonlinearity between the wire temperature and the output angle. Further, we use the following static relationship between the applied current and the wire temperature

$$\tilde{T}_w \stackrel{def}{=} T_w - T_{amb} = \frac{b_1}{a_1} i^2 \tag{47}$$

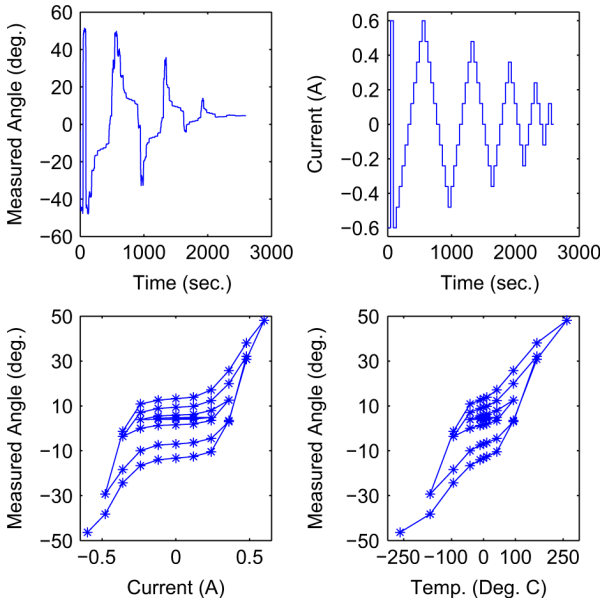


Fig. 6. Measured output, current input, and identified hysteresis.

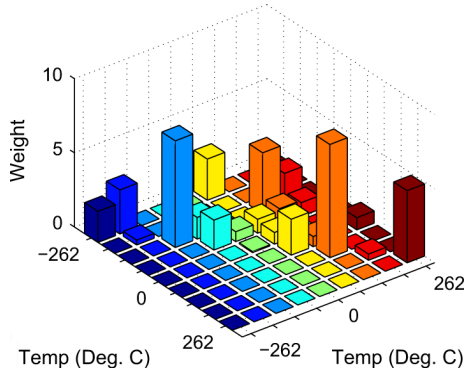


Fig. 7. Identified Preisach weighting masses.

where $T_w$ is the wire temperature, $T_{amb}$ is the ambient temperature, and $a_1 = 0.25$ and $b_1 = 181.56$ are values obtained from the wire's material properties [1]. Heat dynamic models for SMA have been considered in the literature (e.g., [10] and [35]), but the relation (47) proved suitable for testing the multirate scheme. As mentioned above, identification of the Preisach weights was conducted using a constrained least squares algorithm. The measured rotation angle is shown in Fig. 6 (top left); this angle was generated by the supplied current (top right). The identified hysteresis nonlinearity is also illustrated (bottom left). Using the equation $\hat{T}_w = sign(i)b_1 i^2/a_1$ we can construct a Preisach operator that maps the temperature to the measured angle. This map is shown in the bottom right plot of Fig. 6. Note that the sign of the temperature indicates which wire is being heated. The identified Preisach weighting masses are shown in Fig. 7. The following second order transfer function, identified from the joint's frequency response, captures the dynamics:

$$\frac{0.5}{s^2 + 2.25s + 0.5}.$$

To close the loop, we use PID as our sampled-data controller in cascade with the hysteresis inversion operator as in Fig. 2. The computed current $i$ applied to the ZOH is given by $i = sign(v)\sqrt{|v|}$ where $v = k_g \hat{\Gamma}^{-1}[u_e(k), \psi_0]$ and $u_e$ is the PID

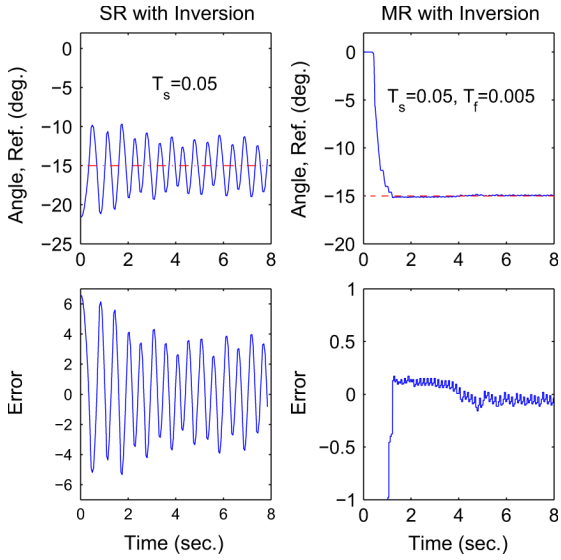


Fig. 8. Angle regulation experimental results for SR (left) and MR (right).

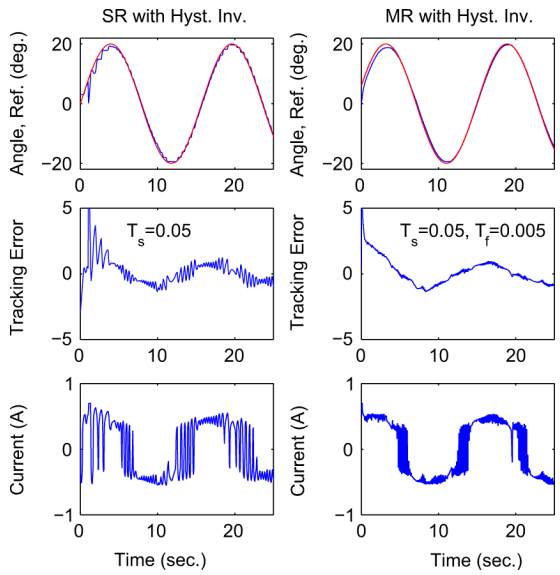


Fig. 9. Tracking experimental results for SR (left) and MR (right).

control. The term $k_g$ is chosen proportional to $a_1/b_1$ and provides an additional degree of freedom in the control design.

The control current is saturated outside $[-0.7,\ 0.7]$ amps. To test the multirate controller, we use the linear discrete-time high-gain observer, (19)–(20) with $\phi_0 = 0$, to estimate the angular velocity of the rotary joint based on the measured rotation angle. The observer parameters are taken to be: $\alpha_1 = 2, \alpha_2 = 1$, and $\varepsilon = T_f/\alpha$, where $\alpha = 0.3$. Fig. 8 shows the results of a regulation experiment where the controller attempts to rotate the joint to an angle of $-15$ degrees and maintain it there. The plot compares the response of a single-rate controller with a sampling period of 0.05 s against the response of the multirate controller where the measurement period was $T_f = 0.005$ s. The PID gains are $k_p = 30$, $k_i = 0.1$, $k_d = 4$ for the proportional, integral, and derivative terms, respectively and $k_g = 0.028$. As can be clearly seen, the single-rate scheme was unable to stabilize the system under this large sampling period. The multirate controller, with the more accurate state estimation, was able to achieve stabilization. Fig. 9 shows a similar result for

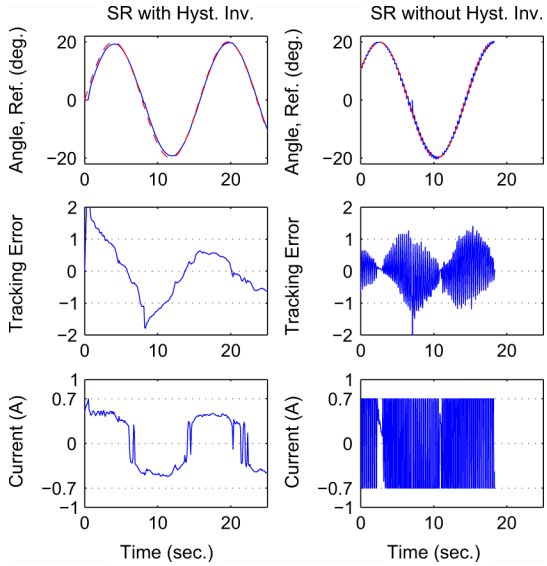


Fig. 10. Comparison of Hysteresis inversion (left) with PID (right).

the tracking problem, where the angular reference is a sinusoid of 0.4 rad/s. For this experiment $k_p = 8$, $k_i = 1$, $k_d = 0.1$, and $k_g = 0.0028$. The plot of the single-rate case exhibits a small oscillation in the response. This behavior can be seen in the current control signal, where it oscillates between positive and negative. Such a control response can prematurely fatigue the SMA wire. The multirate case shows a more satisfactory response. We note that, for the single-rate case, stability can be achieved by faster sampling, but these results demonstrate the added stability for the multirate case with the chosen control sampling rate. Finally, we compare the PID with hysteresis inversion controller to PID without inversion. In both cases we use a single-rate controller with sampling period of 0.01 s and the PID gains were tuned to try and minimize the tracking error at this sampling period. Fig. 10 shows that the controller with hysteresis inversion achieves stable tracking with $k_p = 8$, $k_i = 2$, $k_d = 0.1$, and $k_g = 0.0028$. For the PID case, the response at this sampling period is oscillatory and the control signal continuously saturates. The example shown in the figure corresponds to $k_p = 5$, $k_i = 0$, $k_d = 0.1$. Stabilization is achieved for the PID case with faster sampling, but this comes at the expense of larger control effort than the hysteresis inversion case. Indeed, using a sampling rate of $T_s = 0.005$ s, experiments were conducted where the PID gains were tuned to give a similar tracking performance for the two controllers. Under the PID with hysteresis inversion scheme, a 27% reduction in the R.M.S of the control signal was found when compared to the PID without inversion.

## VI. Conclusion

We have studied multirate sampled-data output feedback control using a discrete-time high-gain observer. Given a sampled-data state feedback controller that, in the presence of bounded disturbances, globally asymptotically stabilizes a set containing the origin, the multirate observer recovers the same set as $\varepsilon \longrightarrow 0$. Moreover, stability is obtained with the same control update rate that was chosen under the state feedback design with a sufficiently fast output sampling rate. This analysis builds on the results of [7] by considering bounded exogenous signals, which were not considered in [7], and allowing the flexibility to separate the control and measurement sampling rates. In the absence of disturbances we were able to show exponential convergence to the origin for the multirate output feedback system given an exponentially stabilizing single-rate state feedback control.

As an application we have considered smart material actuated systems where the closed-loop control is based on hysteresis inversion. Experimental results of a shape memory alloy actuated rotary joint demonstrate the added degree of stability of the multirate scheme over a single-rate scheme under sampling period $T_s$. We have also seen that PID control with hysteresis inversion can provide added stability with lower control effort than with a PID controller alone. For the robotic joint, we have used an empirically-based model similar in structure to Fig. 2. This model proved adequate for testing the multirate output feedback control scheme with hysteresis inversion. The results demonstrate good control performance for the regulation and tracking problems considered.

In addition to the experimental results presented, simulation studies were conducted to examine the effect of peaking on the multirate scheme. In [2] a numerical example highlights some of the stability properties of the multirate output feedback controller and its ability to handle peaking in the estimates. There it was seen that the multirate scheme is less sensitive to the peaking phenomenon then the single-rate scheme. That is, in the presence of an impulsive-like disturbance that may occur at any time, the control signal did not saturate as easily under the multirate scheme compared to the single-rate scheme.

## Appendix I
## Proof of Theorem 1

First, consider the closed-loop system under sampled-data state feedback (12)–(13). From Assumption 4 and the discrete-time converse Lyapunov theorem of [16] there is a smooth Lyapunov function $V(k, \chi_a)$ that depends on $T_s$ and satisfies (15)–(16). Let $\Omega_1$ denote the compact set $\{V(k, \chi_a) \leq c_1\}$. We choose $c_1 > \max_{\chi_a \in \mathcal{M}} V(k, \chi_a)$ so that $\mathcal{M}$ is in the interior of $\Omega_1$. We take $W(\xi) = \xi^T P \xi$ as the Lyapunov function for the observer error dynamics where $P$ is positive definite and satisfies $A_f^T P A_f - P = -I$. Also, from ([28, Ch. 23, Th. 23.7]) we have that $\|P\| > 1$ . Consider the sets $\Omega_2 = \{V(k, \chi_a) \leq c_2\}$, $\Lambda_1 = \Omega_2 \times \{W(\xi) \leq c_3 \varepsilon^2\}$ where $c_3 > 0$ and $\Omega_2$ is a compact subset of $\mathbb{R}^\ell$ for any $c_2 > 0$. We take $c_2^s > c_1^s > c_2 > c_1$ so that $\mathcal{M} \subset \Omega_1 \subset \Omega_2 \subset \Omega_1^s \subset \Omega_2^s$ (defined in 17) and we show that for $\chi_a(0)$ starting in $\mathcal{M}$, $\chi_a(k)$ remains in $\Omega_2$. Due to the boundedness of $\gamma$ and $\mathcal{G}_d$ in $\hat{x}$ we have $\|\mathcal{F}(k, \chi_a, \hat{x}_s, d, \gamma(\vartheta, \hat{x}_s, \zeta, d) + e, T_s)\| \leq K_1$ and $\|\mathcal{G}_d(n, \chi, \xi, d, \zeta, u, \varepsilon)\| \leq K_2$ for all $(\chi_a, \xi) \in \Omega_1 \times \mathbb{R}^r$ where $K_1$ and $K_2$ are positive constants independent of $\varepsilon$. Using (7) it is straightforward to show that the exact discrete-time model for (6) is locally Lipschitz in $\chi$ with Lipschitz constant $e^{L_1 T_s}$. Further, letting $L_4$ be the Lipschitz constant of $f$ with respect to $u$, the exact discrete-time model for (6) is locally Lipschitz in $u$ with Lipschitz constant $L_4 T_s$. Using this fact and Assumption 3 we conclude that $\mathcal{F}$ is locally Lipschitz in

$(\chi_a, \hat{x}_s, u)$. Considering (11), (23), and (29) along with the Lipschitz continuity of $\mathcal{F}$ and $\gamma$ we have that

$$\begin{aligned}&\|\mathcal{F}(k,\chi_a,\hat{x}_s,d,\gamma(\vartheta,\hat{x}_s,\zeta,d)+e,T_s)\\&\quad-\mathcal{F}(k,\chi_a,x,d,\gamma(\vartheta,x,\zeta,d)+e,T_s)\|\\&\leq\varepsilon K_3\|\chi_a\|+K_4\|\xi_s\|\end{aligned}$$

for all $(\chi_a, \xi_s) \in \Lambda_1$ and for some positive constants $K_3$ and $K_4$ dependent on $T_s$, but independent of $\varepsilon$. From the foregoing, it can be shown that in the set $\Lambda_1$

$$\begin{aligned}&V(k+1,\chi_a(k+1))\\&\quad=V(k+1,\mathcal{F}(k,\chi_a,\hat{x}_s,d,\gamma(\vartheta,\hat{x}_s,\zeta,d)+e,T_s))\\&\quad\leq V(k,\chi_a(k))-U_3(|\chi_a(k)|_{\mathcal{A}})+\varepsilon K_5(T_s)\end{aligned}\tag{48}$$

for some positive constant $K_5(T_s)$ that depends on $T_s$. We can choose $\varepsilon$ small enough that $\chi_a(k) \in \{V(k,\chi_a(k)) \leq c_1\}$ cannot leave $\Omega_2$. This can be seen from $V(k+1,\chi_a(k+1)) \leq c_1 + \varepsilon K_5(T_s) < c_2$ for $V(k,\chi_a(k)) \leq c_1$, $\varepsilon < \varepsilon_1 \stackrel{def}{=} (c_2 - c_1)/K_5(T_s)$. Likewise, for $c_1 \leq V(k,\chi_a(k)) \leq c_2$ we have $V(k+1,\chi_a(k+1)) \leq c_2 - K_6 + \varepsilon K_5(T_s) < c_2$ for $\varepsilon < \varepsilon_2 \stackrel{def}{=} K_6/K_5(T_s)$ where

$$K_6 = \min_{c_1 \leq V(k,\chi_a(k)) \leq c_2} U_3(|\chi_a(k)|_{\mathcal{A}}).$$

Thus, $\Omega_2$ is positively invariant. For the observer error dynamics (26), we can arrive at

$$W(\xi(n+1)) \leq \left(1-\frac{1}{\|P\|}\right) W(\xi(n))+\varepsilon K_7\|\xi(n)\|+\varepsilon^2 K_8 \tag{49}$$

where $K_7 = 2K_2\|P\|\|A_f\|$ and $K_8 = K_2^2\|P\|$. For $\xi(n) \in \{W(\xi(n)) \leq c_3\varepsilon^2\}$, we obtain

$$W(\xi(n+1)) \leq \left(1-\frac{1}{\|P\|}\right) c_3\varepsilon^2+\varepsilon^2 K_7\sqrt{\frac{c_3}{\lambda_{\min}(P)}}+\varepsilon^2 K_8.$$

It can be seen that for $c_3$ large enough, $W(\xi(n+1)) \leq c_3\varepsilon^2$. Therefore, $\Lambda_1$ is positively invariant.

With the initial conditions $(\chi_a(0), \hat{x}(0)) \in \mathcal{M} \times \mathcal{N}$ we have that $\|\xi(0)\| \leq l/\varepsilon^{r-1}$, where $l$ depends on $\mathcal{M}$ and $\mathcal{N}$. Since $\mathcal{M}$ is in the interior of $\Omega_1$, $\chi_a(0)$ is in $\Omega_1$. From (13), as long as $\chi_a(k) \in \Omega_1$, then

$$\|\chi_a(k) - \chi_a(0)\| \leq K_9(T_s)k \tag{50}$$

for some positive constant $K_9$ dependent on $T_s$. Hence, $\chi_a(k)$ remains in $\Omega_1$ for $k \leq K_{10}$ for some positive constant $K_{10}$. With $\chi_a(k) \in \Omega_1$ and $\xi \notin \{W(\xi) \leq c_3\varepsilon^2\}$, we can rewrite (49) as

$$\begin{aligned}W(\xi(n+1)) \leq{}& \left(1-\frac{1}{2\|P\|}\right) W(\xi(n))\\&-\frac{1}{2\|P\|}W(\xi(n))+\varepsilon K_7\sqrt{\frac{W(\xi(n))}{\lambda_{\min}(P)}}+\varepsilon^2 K_8.\end{aligned}$$

Then for $W(\xi) \geq c_3\varepsilon^2$, we can choose $c_3$ large enough that $W(\xi(n+1)) \leq \lambda W(\xi(n))$ for $0 < \lambda = (1 - 1/(2\|P\|)) < 1$. Hence

$$W(\xi(n)) \leq \lambda^n\|P\|\frac{l^2}{\varepsilon^{2r-2}}.\tag{51}$$

And $\xi$ enters $\{W(\xi) \leq c_3\varepsilon^2\}$ for $\lambda^n\|P\|l^2/\varepsilon^{2r-2} \leq \varepsilon^2 c_3$. To show boundedness of trajectories, let

$$\bar{n}(\varepsilon) = \frac{ln\left(\frac{\|P\|l^2}{c_3\varepsilon^{2r}}\right)}{ln\left(\frac{1}{\lambda}\right)}\tag{52}$$

and note that $\xi \in \{W(\xi) \leq c_3\varepsilon^2\}$ for all $n \geq \bar{n}(\varepsilon)$. From (50), $\chi_a(k) \in \Omega_1$ for all $k \leq K_{10}$. We can select $\varepsilon_3$ such that for all $0 < \varepsilon \leq \varepsilon_3$, $T_f\bar{n}(\varepsilon) < T_s k \leq T_s K_{10}$. This can be seen by using (52) to obtain $\varepsilon\alpha ln(\|P\|l^2/(c_3\varepsilon^{2r})) < K_{10}T_s ln(1/\lambda)$ where the left-hand side tends to zero as $\varepsilon \to 0$. This $\varepsilon_3$ ensures that $\xi(n)$ enters the set $\{W(\xi) \leq c_3\varepsilon^2\}$ before $\chi_a(k)$ leaves $\Omega_1$. Thus, $\chi_a(k)$ is bounded for all $k \geq 0$. The trajectory $\xi(n)$ enters the set $\{W(\xi) \leq c_3\varepsilon^2\}$ during the time period $[0, \lceil\bar{n}(\varepsilon)\rceil]$ (where the notation $\lceil\bar{n}\rceil$ denotes the largest integer greater than or equal to $\bar{n}$) and remains there for all $n \geq \bar{n}(\varepsilon)$. Furthermore, it is bounded by (51) prior to entering this set. Now, since $\chi_a(k) \in \Omega_2$ which is a subset of $\Omega_2^s$ we can apply (8) and (23) to show that all closed-loop trajectories are bounded by choosing $\varepsilon_1^* = \min(\varepsilon_1, \varepsilon_2, \varepsilon_3)$. From the boundedness of $\chi(k)$, $d(k)$, and $u(k)$ and using (8), it can be seen that there exist a $\delta(T_s)$ where $\delta(T_s) \to 0$ as $T_s \to 0$ satisfying (31).

Ultimate boundedness follows by an argument similar to [7]. Indeed since $\xi(n) \in \{W(\xi(n)) \leq c_3\varepsilon^2\}$, then given any $\nu > 0$ we can find $\varepsilon_4$ dependent on $\nu$ such that $\|\xi(n)\| \leq 1/2\nu$ for all $n \geq \bar{n}(\varepsilon)$ and all $0 < \varepsilon \leq \varepsilon_4$. Now, consider the compact set $\{U_3(|\chi_a(k)|_{\mathcal{A}}) \leq 2\varepsilon K_5(T_s)\}$ and let

$$\omega_1(\varepsilon) = \max_{U_3(|\chi_a(k)|_{\mathcal{A}}) \leq 2\varepsilon K_5(T_s)} V(k,\chi_a)$$

and note that $\omega_1(\varepsilon) \to 0$ as $\varepsilon \to 0$. We have that the set $\{V(k,\chi_a) \leq \omega_1(\varepsilon)\}$ is compact and $\{U_3(|\chi_a(k)|_{\mathcal{A}}) \leq 2\varepsilon K_5(T_s)\} \subset \{V(k,\chi_a) \leq \omega_1(\varepsilon)\}$. Rewrite (48) as

$$\begin{aligned}V(k+1,\chi_a(k+1)) \leq{}& V(k,\chi_a(k))\\&-\frac{1}{2}U_3(|\chi_a(k)|_{\mathcal{A}})-\left(\frac{1}{2}U_3(|\chi_a(k)|_{\mathcal{A}})-\varepsilon K_5(T_s)\right).\end{aligned}$$

Therefore, with $V(0,\chi_a(0)) \geq \omega_1(\varepsilon)$, we have that

$$V(k+1,\chi_a(k+1)) \leq V(0,\chi_a(0))-\sum_{i=0}^{k}\frac{1}{2}U_3(|\chi_a(i)|_{\mathcal{A}})$$

whenever $V(k,\chi_a(k)) \geq \omega_1(\varepsilon)$. Further, $V(k+1,\chi_a(k+1)) \leq V(0,\chi_a(0))-\varepsilon K_5(T_s)(k+1)$. Thus there exists a finite time $k^*$ such that $\chi_a(k^*)$ enters the set $\{V(k,\chi_a) \leq \omega_1(\varepsilon)\}$. Now, consider the time $k \geq k^*$. For $\chi_a(k) \in \{V(k,\chi_a) \leq \omega_1(\varepsilon)\}$ and $U_3(|\chi_a(k)|_{\mathcal{A}}) > 2\varepsilon K_5(T_s)$ we obtain $V(k+1,\chi_a(k+1)) \leq \omega_1(\varepsilon)-U_3(|\chi_a(k)|_{\mathcal{A}})/2 < \omega_1(\varepsilon)$. Therefore, $\chi_a(k+1)$ remains in the set $\chi_a(k) \in \{V(k,\chi_a) \leq \omega_1(\varepsilon)\}$. On the other hand, for $\chi_a(k) \in \{V(k,\chi_a) \leq \omega_1(\varepsilon)\}$ and $U_3(|\chi_a(k)|_{\mathcal{A}}) \leq 2\varepsilon K_5(T_s)$ we have $V(k+1,\chi_a(k+1)) \leq \omega_1(\varepsilon) + \varepsilon K_5(T_s) \stackrel{def}{=} \omega_2(\varepsilon)$.

Hence, $\chi_a(k+1)$ may leave $\{V(k,\chi_a) \le \omega_1(\varepsilon)\}$ but remains in a set defined by $\{V(k,\chi_a) \le \omega_2(\varepsilon)\}$ where $\omega_2(\varepsilon) \to 0$ as $\varepsilon \to 0$. Now, for $\chi_a(k)$ in the set $\{\omega_1(\varepsilon) < V(k,\chi_a) \le \omega_2(\varepsilon)\}$, we have $U_3(|\chi_a(k)|_{\mathcal{A}}) > 2\varepsilon K_5(T_s)$. Therefore $V(k+1,\chi_a(k+1)) \le V(k,\chi_a(k)) - U_3(|\chi_a(k)|_{\mathcal{A}})/2 < \omega_2(\varepsilon)$. Thus, $V(k+1,\chi_a(k+1)) \le \omega_2(\varepsilon)$, $\forall k \ge k^*$. In other words, for $\chi_a(k)$ belonging to the set $\{V(k,\chi_a) \le \omega_1(\varepsilon)\}$ at time $k = k^*$, then $\chi_a(k)$ must be in the set $\{V(k,\chi_a) \le \omega_2(\varepsilon)\}$ for all $k \ge k^*+1$. From (15) $|\chi_a(k)|_{\mathcal{A}} \le U_1^{-1}(\omega_2(\varepsilon))$ for all $k \ge k^*+1$. Using this we can find an $\varepsilon_5$ dependent on $\nu$ such that $|\chi_a(k)|_{\mathcal{A}} \le \nu/2$ for all $0 < \varepsilon \le \varepsilon_5$ and all $k \ge k_1^*$ for a finite time $k_1^*$. From the foregoing, we obtain (30) where $\varepsilon_2^* = \min(\varepsilon_4, \varepsilon_5)$. ◁

## Appendix II
## Proof of Theorem 2

We study the closed-loop system in the slow sample time $k$ and show that the discrete-time trajectories converge exponentially to the origin. To do so, we will need a description of (34) in the slow sampling time $k$. We note that the ratio of the sampling rates $h = T_s/T_f$ is taken to be a positive integer. Also, we will work locally, so consider a ball $B(0,\varrho_1)$ of radius $\varrho_1 > 0$ around the origin $(\chi,\xi) = (0,0)$. The results of the Theorem 1 guarantee that for $\varepsilon$ small enough, the trajectories will enter this set in finite time. Furthermore, the functions $f(\chi,0,u)$ and $\gamma(x,\zeta)$ are continuously differentiable in a neighborhood of the origin. We begin by studying (34) over one slow time period $[k,k+1]$. Consider the discrete-time state (33) and the estimation error dynamics in the fast sampling time $n$

$$\chi(n+1) = \chi(n) + T_f f(\chi(n),0,u(k)) + T_f^2 \Phi_0(\chi(n),u(k),T_f) \quad (53)$$

$$\xi(n+1) = A_f \xi(n) + \varepsilon \mathcal{G}_0(\chi(n),\xi(n),0,\zeta(k),u(k),\varepsilon). \quad (54)$$

Performing the accumulation of (54) over the interval $hk \le n \le h(k+1)$ it is not clear that the right-hand-side converges to an $O(\varepsilon)$. To show this, we will use a change of variables. First, we note that (53)–(54) has a two-time scale behavior. For (54), we have the quasi-steady-state relation $\xi(n) = A_f\xi(n) + \varepsilon\mathcal{G}_0(\chi(n),\xi(n),0,\zeta(k),u(k),\varepsilon)$. We seek a solution to the above equation in the form $\xi(n) = \varphi(\chi(n),\zeta(k),u(k),\varepsilon)$ where $\varphi$ is a continuously differentiable function of its arguments and $\varphi(0,0,0,0) = 0$. This equation describes an $(r+s)$-dimensional manifold in the $(2r+s)$-dimensional state space of $(\chi,\xi)$ and is called the slow manifold of (53) and (54). Evaluating $\xi(n) = \varphi(\chi(n),\zeta(k),u(k),\varepsilon)$ at $n+1$ and substituting the difference (53) and (54) results in the following manifold condition:

$$\begin{aligned} &A_f\varphi(\chi(n),\zeta(k),u(k),\varepsilon) \\ &\quad -\varphi(\chi(n) + T_f f(\chi(n),0,u(k)) \\ &\quad +\varepsilon\mathcal{G}_0\left(\chi(n),\varphi(\chi(n),\zeta(k),u(k),\varepsilon)\right),0,\zeta,u,\varepsilon) \\ &\quad +T_f^2\Phi_0(\chi(n),u(k),T_f),\zeta(k),u(k),\varepsilon) = 0. \end{aligned} \quad (55)$$

Setting $\varepsilon = 0$ we have

$$(I - A_f)\varphi(\chi(n),\zeta(k),u(k),0) = 0. \quad (56)$$

Because $|\lambda(A_f)| < 1$, $(I - A_f)$ is nonsingular. Therefore, $\varphi(\chi,\zeta,u,0) = 0$. Using the implicit function theorem ([34]) we have that $\varphi(\chi,\zeta,u,\varepsilon)$ satisfies (55) for $\varepsilon$ sufficiently small. Furthermore, due to (56) this function is $O(\varepsilon)$. Consider now the change of variables

$$\eta(n) = \xi(n) - \varphi(\chi(n),\zeta(k),u(k),\varepsilon) \quad (57)$$

which along with (55) results in

$$\begin{aligned} &\eta(n+1) \\ &\quad = A_f\eta(n) + \varepsilon[\mathcal{G}_0(\chi(n),\eta(n) \\ &\qquad +\varphi(\chi(n),\zeta(k),u(k),\varepsilon),0,\zeta(k),u(k),\varepsilon) \\ &\qquad -\mathcal{G}_0\big(\chi(n),\varphi(\chi(n),\zeta(k),u(k),\varepsilon), \\ &\qquad\quad 0,\zeta(k),u(k),\varepsilon\big)]. \end{aligned} \quad (58)$$

We rewrite the right hand side as

$$\eta(n+1) = A_f\eta(n) + \varepsilon\tilde{\mathcal{G}}\left(\chi(n),\eta(n),\zeta(k),u(k),\varepsilon\right) \quad (59)$$

where $\tilde{\mathcal{G}}\left(\chi(n),0,\zeta(k),u(k),\varepsilon\right) = 0$. Therefore, $\eta = 0$ is an equilibrium point of the transformed system. The function $\tilde{\mathcal{G}}$ is continuously differentiable with convex domain $B(0,\varrho_1)$. From ([17, ex. 3.23, pg. 108]) we have the following relation:

$$\tilde{\mathcal{G}}\left(\chi(n),\eta(n),\zeta(k),u(k),\varepsilon\right) = \int_0^1 \frac{\partial\tilde{\mathcal{G}}}{\partial\eta}(\chi,\sigma\eta,\zeta,u,\varepsilon)d\sigma\,\eta.$$

Define the right-hand side of this equation as

$$\int_0^1 \frac{\partial\tilde{\mathcal{G}}}{\partial\eta}(\chi,\sigma\eta,\zeta,u,\varepsilon)d\sigma\eta \stackrel{def}{=} \tilde{B}(\chi(n),\eta(n),\zeta(k),u(k),\varepsilon)\,\eta.$$

Due to the fact that $\chi$ and $\xi$ are bounded and belong to the set $B(0,\varrho_1)$, we can treat the equation

$$\eta(n+1) = \left[A_f + \varepsilon\tilde{B}(\chi(n),\eta(n),\zeta(k),u(k),\varepsilon)\right]\eta(n) \quad (60)$$

as a time-varying linear system. Let $\tilde{A}(n) = A_f + \varepsilon\tilde{B}(\chi(n),\eta(n),\zeta(k),u(k),\varepsilon)$. Since $|\lambda(A_f)| \le \lambda_1 < 1$ for some positive constant $\lambda_1$, it follows from ([28, Th. 24.7]) that, for $\varepsilon$ sufficiently small, the state transition matrix, $\Phi_{\tilde{A}}(n,n_0)$, of (60) satisfies $\|\Phi_{\tilde{A}}(n,n_0)\| \le \kappa_1\lambda_2^{n-n_0}$ where $0 < \lambda_2 < 1$ and $\kappa_1$ is a positive constant. In addition, it can be shown that there exist $\varepsilon_6$ such that the following properties are satisfied uniformly in $\varepsilon$ for all $0 < \varepsilon \le \varepsilon_6$: $|\lambda(\tilde{A})| \le c_1$, $\|\tilde{A}\| \le c_2$, and $\|\tilde{A}(n) - A_f\| \le c_3\varepsilon$ where $c_1$, $c_2$, and $c_3$ are positive constants. Now let $\Upsilon(n,n_0) = \Phi_{\tilde{A}}(n,n_0) - A_f^{n-n_0}$. It can be shown (by the discrete-time counterpart of [19,Ch 5., Lemma 2.2]) that there exist positive constants $\varepsilon_7$, $\kappa_2$, and $0 < \lambda_3 < 1$ such that for all $0 < \varepsilon \le \varepsilon_7$ we have that $\|\Upsilon(n,n_0)\| \le \varepsilon\kappa_2\lambda_3^{n-n_0}$. From (60) we have $\eta(n) = \left[A_f^{n-n_0} + \Upsilon(n,n_0)\right]\eta(n_0)$. The accumulation over the period $\left[hk \le n \le h(k+1)\right]$ is given by

$$\eta(hk+h) = \left[A_f^h + \Upsilon(hk+h,hk)\right]\eta(hk). \quad (61)$$

Since $h$ is $O(1/\varepsilon)$ and $|\lambda(A_f)| < 1$ we have that $A_f^h = O(\varepsilon)$. Using this and the fact that $\Upsilon$ is $O(\varepsilon)$, we rewrite (61) as $\eta(hk+h) = \varepsilon G(\eta(hk),\chi(hk),\zeta(k),u(k),\varepsilon)$ where the function $G$ is continuously differentiable. We now have an equation that describes the evolution of the estimation error in the slow sample time $k$. Consider the control (23) and (35) and substitute these expressions into (57). We get $\eta(hk) = \xi(hk) - \varphi(\chi(hk),\zeta(k),\gamma([I - \varepsilon N_2]x(hk) + N_1\xi(hk),\zeta(k)),\varepsilon)$. Dropping the $h$ notation, we redefine the right-hand side of the above equation as

$\eta(k) = \xi(k) - \tilde{\varphi}(\chi(k), \xi(k), \varepsilon)$ where $\tilde{\varphi}$ is continuously differentiable. By noting that $\tilde{\varphi} = 0$ for $\varepsilon = 0$, the implicit function theorem shows us that there is an open set $\mathcal{V}$ containing $(\eta, \xi, \varepsilon) = 0$ such that

$$\xi(k) = \varpi(\eta(k), \chi(k), \varepsilon) \tag{62}$$

where the function $\varpi$ is continuously differentiable in $\mathcal{V}$. From the ultimate boundedness of Theorem 1, we can choose $\varepsilon$ small enough to guarantee that we are in $\mathcal{V}$. Let $\mathcal{F}(\chi_a(k), \xi_s(k), T_s, \varepsilon)$ denote the right-hand side of (32)–(33) where $\chi_a = (\vartheta, \chi)$ and $\hat{x}_s$ and $u$ are given by (35) and (23), respectively. Using (62) we write the closed-loop system in the slow sample time in terms of $\chi_a$ and $\eta$ as

$$\chi_a(k+1) = \mathcal{F}(\chi_a(k), \varpi(\eta(k), \chi_a(k), \varepsilon), T_s, \varepsilon) \tag{63}$$
$$\eta(k+1) = \varepsilon G(\eta(k), \chi_a(k), \zeta(k), \varepsilon). \tag{64}$$

Using (63) and (64) through the change of variables (57) we can show that all closed-loop trajectories exponentially converge to the origin. To do this we begin by setting $\eta = 0$ and $\varepsilon = 0$ in (63). This results in the reduced system $\chi_a(k+1) = \mathcal{F}(\chi_a(k), 0, T_s, 0)$, which is the closed-loop system under sampled-data state feedback. Linearizing about $\chi_a = 0$ we obtain $\chi_a(k+1) = A_{11}\chi_a(k)$ where $|\lambda(A_{11})| < 1$ by hypothesis. Next, we linearize the full system (63)–(64) about $(\chi_a, \eta) = (0, 0)$ to obtain

$$\begin{aligned}\chi_a(k+1) &= (A_{11} + \varepsilon A_{12})\chi_a(k) + A_{13}\eta(k) \\ &\quad + T_s g_1(\chi_a, \eta, T_s, \varepsilon) \qquad (65)\\ \eta(k+1) &= \varepsilon A_{21}\chi_a(k) + \varepsilon A_{22}\eta(k) + \varepsilon g_2(\eta, \chi_a, \varepsilon) \qquad (66)\end{aligned}$$

where $g_1$ and $g_2$ are continuous functions. We have that for any $\gamma_1 > 0$ and $\gamma_2 > 0$ there exist $\varrho_2 > 0$ such that $\|g_1\|_2 < \gamma_1\|(\chi_a, \eta)\|_2$ and $\|g_2\|_2 < \gamma_2\|(\chi_a, \eta)\|_2$ for all $\|(\chi_a, \eta)\|_2 < \varrho_2$. Since $\tilde{\varphi}$ is continuous, we can choose $\varrho_1$ so that $(\chi_a, \xi) \in B(0, \varrho_1)$ implies $\|(\chi_a, \eta)\|_2 < \varrho_2$ through the change of variables $\eta = \xi - \tilde{\varphi}$. We need to weaken the variable $\eta$ in the linear part of (65). This is accomplished by choosing a matrix $Q$ that satisfies $(A_{11} + \varepsilon A_{12})Q + A_{13} - \varepsilon Q A_{21} Q - \varepsilon Q A_{22} = 0$. Now, consider the composite Lyapunov function $V(\chi_a(k), \eta(k)) = [\chi_a - Q\eta]^T P_{11}[\chi_a - Q\eta] + \theta\eta^T\eta$ where the matrix $P_{11}$ is positive definite and satisfies $A_{11}^T P_{11} A_{11} - P_{11} = -I$. It can be shown that there is $\theta$ sufficiently large and $\varepsilon_8$ sufficiently small such that the following holds uniformly in $\varepsilon$ for all $0 < \varepsilon \le \varepsilon_8$: $\delta_1\|(\chi_a, \eta)\|^2 \le V \le \delta_2\|(\chi_a, \eta)\|^2$ where $\delta_1, \delta_2$ are positive constants. We have $\Delta V \le -\mathcal{Y}^T\Pi\mathcal{Y}$ where

$$\mathcal{Y} = \begin{bmatrix} \|\chi_a(k) - Q\eta(k)\| \\ \|\eta(k)\| \end{bmatrix}, \quad \Pi = \begin{bmatrix} \pi_1 & \pi_2 \\ \pi_2 & \pi_3 \end{bmatrix}$$

$$\begin{aligned}\pi_1 &= 1 - \varepsilon[\beta_1 + \beta_2\gamma_1 + \beta_3\gamma_1 + \beta_4\gamma_1\gamma_2] \\ &\quad - \varepsilon^2[\theta h_1(\gamma_2) + h_2(\gamma_2)] - \beta_5\gamma_1 - \beta_6\gamma_1^2 \\ \pi_2 &= -\theta\varepsilon^2[\beta_7 + \beta_8\gamma_2] - \varepsilon^2\beta_9\gamma_2 \\ &\quad - \varepsilon[\beta_{10}\gamma_1 + \beta_{11}\gamma_2 + \beta_{12}\gamma_1\gamma_2] - \beta_{13}\gamma_1 \\ \pi_3 &= \theta - \theta\varepsilon^2 h_3(\gamma_2) - \varepsilon^2\beta_{14}\gamma_2^2 - \varepsilon\beta_{15}\gamma_1\gamma_2 - \beta_{16}\gamma_1^2\end{aligned}$$

for some positive constants $\beta_i$ that, in general, depend on $T_s$ and for functions $h_1$, $h_2$, and $h_3$ that are quadratic polynomial functions of $\gamma_2$. From the foregoing it can be shown that there exist $\gamma_1^*(T_s)$, dependent on $T_s$ but independent of $\varepsilon$ and $\theta$, sufficiently small; $\theta^*(\gamma_1, T_s)$, dependent on $\gamma_1$ but independent of $\varepsilon$, sufficiently large; and $\varepsilon_9(\theta, \gamma_1, \gamma_2, T_s)$ dependent on $\theta$, $\gamma_1$, and $\gamma_2$ such that for all $0 < \gamma_1 \le \gamma_1^*$, $\theta \ge \theta^* > 0$, and $0 < \varepsilon \le \varepsilon_9$ the matrix $\Pi$ is positive definite. Therefore, from the ultimate boundedness of $\chi_a$ and $\xi$ we have that $\|\mathcal{Y}(k)\| \le C_1\lambda_4^{(k-k_2^*)}$ for all $k \ge k_2^*$ where $k_2^*$ is some positive integer and $C_1$ and $\lambda_4 < 1$ are positive constants. In the absence of the time varying disturbance $d$, the inequality (8) reduces to

$$\|\chi(t) - \chi(k)\| \le \frac{1}{L_1}\left[e^{(t-kT_s)L_1} - 1\right]\|f(\chi(k), 0, u(k))\|$$

for all $t \in [kT_s, kT_s + T_s]$. Using this, the control (23), and (35) it can be shown that $\|\chi(t)\| \le C_2 e^{-a^*(t - k_2^* T_s)}$, $\forall t \ge k_2^* T_s$ for some positive constant $C_2$ and $a^* = ln(1/(\lambda_4)^{(1/T_s)})$, where $a^* > 0$ since $\lambda_4 < 1$. From the boundedness of $\chi(t)$ for all $t \ge 0$, it can be shown that $\chi(t)$ is exponentially convergent for all $0 < \varepsilon \le \varepsilon_3^* = \min\{\varepsilon_2^*, \varepsilon_6, \varepsilon_7, \varepsilon_8, \varepsilon_9\}$. ◁

## REFERENCES


[1] J. H. Ahrens, "Design and Performance Tradeoffs of High-Gain Observers with Applications to Smart Material Actuated Systems," Ph.D. dissertation, Michigan State Univ., East Lansing, MI, 2006.

[2] J. H. Ahrens and H. K. Khalil, "Multirate sampled-data output feedback using high-gain observers," in *Proc. IEEE Conf. Decision Control*, San Diego, CA, Dec. 2006, pp. 4885–4890.

[3] H. Ashrafiuon, M. Eshraghi, and M. H. Elahinia, "Position control of a three-link shape memory alloy actuated robot," *J. Intell. Mater. Syst. Struct.*, vol. 17, pp. 381–392, 2006.

[4] K. J.Åström and B. Wittenmark, *Computer Controlled-Systems: Theory and Design*, third ed. Upper Saddle river, NJ: Prentice Hall, 1998.

[5] J. P. Barbot, S. Monaco, and D. Normand-Cyrot, "Discrete-time approximated linearization of SISO systems under output feedback," *IEEE Trans. Autom. Control*, vol. 44, no. 9, pp. 1729–1733, Sep. 1999.

[6] Z. Chen, X. Tan, and M. Shahinpoor, "Quasi-static positioning of ionic polymer-metal composite (IPMC) actuators," in *Proc. IEEE/ASME Int. Conf. Adv. Intell. Mechatron.*, Monterey, CA, 2005, pp. 60–65.

[7] A. M. Dabroom and H. K. Khalil, "Output feedback sampled-data control of nonlinear systems using high-gain observers," *IEEE Trans. Autom. Control*, vol. 46, no. 11, pp. 1712–1725, Nov. 2001.

[8] C. A. Dickinson and J. T. Wen, "Feedback control using shape memory alloy actuators," *J. Intell. Mater. Syst. Struct.*, vol. 9, pp. 242–250, 1998.

[9] T. W. Duering, K. N. Melton, D. Stöckel, and C. M. Wayman, *Engineering Aspects of Shape Memory Alloys*. London, U.K.: Butterworth-Heinemann, 1990.

[10] M. H. Elahinia, M. Ahmadian, and H. Ashrafiuon, "Design of a kalman filter for rotary shape memory alloy actuators," *Smart Mater. Struct.*, vol. 13, pp. 691–697, 2004.

[11] F. Esfandiari and H. K. Khalil, "Output feedback stabilization of fully linearizable systems," *Int. J. Contr.*, vol. 56, pp. 1007–1037, 1992.

[12] R. B. Gorbet, K. A. Morris, and D. W. L. Wang, "Passivity-based stability and control of hysteresis in smart actuators," *IEEE Trans. Control Syst. Techol.*, vol. 9, no. 1, pp. 5–16, Jan. 2001.

[13] R. B. Gorbet, D. W. L. Wang, and K. A. Morris, "Preisach model identification of a two-wire SMA actuator," in *Proc. IEEE Int. Conf. Robot. Autom.*, Leuven, Belgium, May 1998, pp. 2161–2167.

[14] M. Hashimoto, M. Takeda, H. Sagawa, I. Chiba, and K. Sato, "Application of shape memory alloy to robotic actuators," *J. Robot. Syst.*, vol. 2, pp. 3–25, 1985.

[15] L. Hou, A. N. Michel, and H. Ye, "Some qualitative properties of sampled-data control systems," *IEEE Trans. Autom. Control*, vol. 42, no. 12, pp. 1721–1725, Dec. 1997.

[16] Z. P. Jiang and Y. Wang, "A converse lyapunov theorem for discrete-time systems with disturbances," *Syst. Control Lett.*, vol. 45, pp. 49–58, 2002.

[17] H. K. Khalil, *Nonlinear Systems*, 3 ed. Upper Saddle River, NJ: Prentice Hall, 2002.

[18] H. K. Khalil, "Performance recovery under output feedback sampled-data stabilization of a class of nonlinear systems," *IEEE Trans. Autom. Control*, vol. 49, no. 12, pp. 2173–2184, Dec. 2004.
[19] P. V. Kokotović, H. K. Khalil, and J. O'Reilly, *Singular Perturbations Methods in Control: Analysis and Design*. New York: Academic Press, 1999.
[20] D. S. Laila, D. Nešić, and A. R. Teel, "Open and closed loop dissipation inequalities under sampling and controller emulation," *Eur. J. Control*, vol. 8, pp. 109–125, 2002.
[21] S. Majima, K. Kodama, and T. Hasegawa, "Modeling of shape memory alloy actuator and tracking control system with the model," *IEEE Trans. Control Syst. Tech.*, vol. 9, no. 1, pp. 54–59, Jan. 2001.
[22] I. D. Mayergoyz, *The Preisach Model for Hysteresis*. Berlin, Germany: Springer-Verlag, 1991.
[23] P. E. Moraal and J. W. Grizzle, "Observer design for nonlinear systems with discrete-time measurements," *IEEE Trans. Autom. Control*, vol. 40, no. 3, pp. 395–404, Mar. 1995.
[24] D. Nešić and D. S. Laila, "A note on input-to-state stabilization for nonlinear sampled-data systems," *IEEE Trans. Autom. Control*, vol. 47, no. 7, pp. 1153–1158, Jul. 2002.
[25] D. Nešić and A. R. Teel, "A framework for stabilization of nonlinear sampled-data systems based on their approximate discrete-time model," *IEEE Trans. Autom. Control*, vol. 49, no. 7, pp. 1103–1122, Jul. 2004.
[26] D. Nešić, A. R. Teel, and P. V. Kokotović, "Sufficient conditions for stabilization of sampled-data nonlinear systems via discrete-time approximations," *Syst. Control Lett.*, vol. 38, pp. 259–270, 1999.
[27] I. G. Polushin and H. J. Marquez, "Multirate versions of sampled-data stabilization of nonlinear systems," *Automatica*, vol. 40, pp. 1035–1041, 2004.
[28] W. J. Rugh, *Linear Systems Theory*, second ed. Upper Saddle River, NJ: Prentice Hall, 1996.
[29] I. A. Shkolnikov, Y. B. Shtessel, and S. V. Plekhanov, "Multi-rate digital design for sliding-mode-observer-based feedback control," in *Proc. Amer. Control Conf.*, Portland, OR, 2005, pp. 2427–2432.
[30] X. Tan and J. S. Baras, "Modeling and control of hysteresis in magnetostrictive actuators," *Automatica*, vol. 40, pp. 1469–1480, 2004.
[31] A. R. Teel, D. Nešić, and P. V. Kokotović, "A note on input-to-state stability of sampled-data nonlinear systems," in *Proc. IEEE Conf. Decision Control*, Tampa, FL, Dec. 1998, pp. 2473–2487.
[32] R. Venkataraman and P. S. Krishnaprasad, "Approximate inversion of hysteresis: Theory and numerical results," in *Proc. IEEE Conf. Decision Control*, Sydney, Australia, Dec. 2000, pp. 4448–4454.
[33] A. Visintin, *Differential Models of Hysteresis*. Berlin, Germany: Springer, 1994.
[34] W. R. Wade, *An Introduction to Analysis*, second ed. Upper Saddle River, NJ: Prentice Hall, 2000.
[35] G. V. Webb, D. C. Lagoudas, and A. J. Kurdila, "Hysteresis modeling of SMA actuators for control applications," *J. Intell. Mater. Syst. Struct.*, vol. 9, pp. 432–448, 1998.

**J. Ahrens** (S'01–M'06) was born in Edina, MN, in 1976. He received the B.S. degree in electrical engineering from Cleveland State University, Cleveland, OH, in 1999, and the M.S. and Ph.D. degrees in electrical engineering from Michigan State University, East Lansing, MI, in 2002 and 2006, respectively.

He has been working as a Research Engineer at Corning, Inc., Corning, NY, since 2006. His research interests include nonlinear control theory as well as control-oriented modeling and controller design for large-scale industrial processes and diesel automotive emission systems.

**Xiaobo Tan** (S'97–M'02) received the B.S. and M.S. degrees in automatic control from Tsinghua University, Beijing, China, in 1995 and 1998, respectively, and the Ph.D. degree in electrical and computer engineering from the University of Maryland, College Park, in 2002.

From September 2002 to July 2004, he was a Research Associate with the Institute for Systems Research, University of Maryland. Since August 2004, he has been an Assistant Professor in the Department of Electrical and Computer Engineering and Director of Smart Microsystems Laboratory, Michigan State University, East Lansing. He is an Associate Editor of *Automatica*. His current research interests include electroactive polymer sensors and actuators, modeling and control of smart materials, biomimetic robotics, bio/micromanipulation, and collaborative control of autonomous systems.

Dr. Tan received the National Science Foundation (NSF) CAREER Award in 2006. He was a Guest Editor of the IEEE CONTROL SYSTEMS MAGAZINE for its February 2009 special issue on modeling and control of hysteresis. He is a member of the IEEE Control Systems Society Conference Editorial Board.

**H. Khalil** (S'77–M'78–SM'85–F'89) received the B.S. and M.S. degrees from Cairo University, Cairo, Egypt, and the Ph.D. degree from the University of Illinois, Urbana-Champaign, all in electrical engineering.

Since 1978, he has been with Michigan State University, East Lansing, where he is currently University Distinguished Professor. He consulted for General Motors and Delco Products, and published several papers on singular perturbation methods and nonlinear control. He is the author of *Nonlinear Systems* (Englewood Cliffs, NJ: Prentice Hall 2002) and coauthor of *Singular Perturbation Methods in Control: Analysis and Design* (Philadelphia, PA: SIAM 1999). He was an Associate Editor for *Automatica* and *Neural Networks*, and the Editor of *Automatica* for nonlinear systems and control.

Dr. Khalil is Fellow of IFAC. He received the 1989 IEEE-CSS Axelby Award, the 2000 AACC Ragazzini Award, the 2002 IFAC Textbook Prize, and the 2004 AACC Hugo Schuck Award. He served as Associate Editor of the IEEE TRANSACTIONS ON AUTOMATIC CONTROL. He was Program Chair of the 1988 ACC and General Chair of the 1994 ACC.